16th World Conference on Earthquake, 16WCEE 2017
Santiago Chile, January 9th to 13th 2017
Paper N° 3988
Registration Code: S-N1465509242

Acceleration Response Spectrum: Revisited for Higher Mode Effects

S. Günay[(1)], K. M. Mosalam[(2)]

[(1)] Project Scientist, University of California, Berkeley, selimgunay@berkeley.edu
[(2)] Taisei Professor of Civil Engineering; Director of the Pacific Earthquake Engineering Research Center, University of California, Berkeley, mosalam@berkeley.edu

Abstract

Acceleration response spectrum (ARS) is a tool that has conveniently been used in earthquake engineering in the last 75 years. One of the common uses of the response spectrum concept is the identification of higher mode contribution to the structural response. If the spectral acceleration (SA) corresponding to a higher mode (generally the second or third mode) is significantly larger than that of the first mode, the ground motion is accepted to induce higher mode response. However, in general, this interpretation is not necessarily correct because the structural response is usually inelastic and the ARS is obtained from linear elastic single degree of freedom (SDOF) response. ARS for constant base shear capacity coefficient has been developed to consider the inelastic response. However, such spectrum is not useful for higher mode effects identification since the SA for all the periods are bound by the base shear capacity coefficient and it is likely that the SA values corresponding to all the sought modes are the same.

A modified ARS concept is introduced in this paper for a specific base shear coefficient at a desired period. In this modified ARS, a linear elastic SDOF system with a selected period (which generally corresponds to the first mode period) is analyzed with time history analysis. The time of the ground motion at which inelastic response initiates (i.e., the time when the restoring force first exceeds the base shear capacity) is determined from this analysis and the ground motion is redefined as the original ground motion truncated to this time defined by the initiation of inelastic response. Subsequently, the original ARS procedure is followed using the ground motion with truncated duration to obtain the modified ARS, namely the MARS.

A theoretical background information is provided in the first part of the paper to explain why the proposed MARS is expected to produce a better indicator, compared to ARS, for the identification of ground motions leading to higher mode response. Subsequently, the outline for developing MARS is presented and the superiority of MARS in identifying the ground motions with higher mode effect is demonstrated using the results from nonlinear time history analyses conducted on a 35-story tall building.

Keywords: acceleration response spectrum, base shear coefficient, higher mode effects, nonlinear time history analysis, tall building.

1. Introduction

After its first introduction in [1], acceleration response spectrum (ARS) has conveniently been used in earthquake engineering in the last 75 years. One of the common uses of the ARS concept is the identification of higher mode contribution to the structural response. If the spectral acceleration (SA) corresponding to a higher mode (generally the second or third mode) is significantly larger than the first mode SA, that ground motion is accepted to induce higher mode response. However, in general, this interpretation is not necessarily correct because the structural response is usually inelastic and the ARS is obtained from linear elastic single degree of freedom (SDOF) response. The ARS for constant base shear capacity coefficient has been developed to consider the inelastic response [2, 3]. However, such spectrum is not useful for identification of higher mode effects since the SA values for all the periods are bound by the base shear capacity coefficient and it is likely that the SA values corresponding to all the sought modes are the same.

A modified ARS, namely MARS, concept is introduced in this paper for a specific base shear coefficient at a selected period. In the MARS, a linear elastic SDOF system with a selected period (which generally corresponds to the first mode period) is analyzed with time history analysis. The time of the ground motion when the inelastic response initiates (i.e., the time when the restoring force first exceeds the base shear capacity) is determined from this analysis and the ground motion is redefined as the original ground motion truncated to this time defined by the initiation of inelastic response. Subsequently, the original ARS procedure is followed using the ground motion with truncated duration to obtain the MARS.

The ARS and MARS are computed for 40 ground motions to highlight the differences between the two spectra and the differences related to the identification of higher mode response. The ability of the proposed MARS in capturing the higher mode effects is demonstrated by the nonlinear time history analyses (NTHA) conducted on a 35-story tall building.

2. Theoretical Background

The equations of motion governing the response of a linear multi-degree of freedom (MDOF) system to a ground motion excitation at time *t* is represented as follows until inelasticity occurs:

$$\mathbf{m}\ddot{\mathbf{u}}(t)+\mathbf{c}\dot{\mathbf{u}}(t)+\mathbf{k}\,\mathbf{u}(t)=-\mathbf{m}\boldsymbol{\iota}\,\ddot{u}_g(t) \tag{1}$$

where **m**, **c** and **k** are the mass, damping and stiffness matrices, $\ddot{\mathbf{u}}$, $\dot{\mathbf{u}}$, $\mathbf{u}$ are the response acceleration, velocity and displacement vectors, $\boldsymbol{\iota}$ is the influence vector, defined as the vector that represents the displacements of masses resulting from a static application of a unit ground displacement, and $\ddot{u}_g$ is the ground acceleration. The response of this system can conveniently be determined using the modal superposition procedure [4]. In this procedure, any response quantity of the MDOF system at time *t* is obtained by applying the equivalent static force vector $\mathbf{f}(t)$ in Eq. (2) to the structure as a static force and conducting structural analysis to compute the response quantities. Therefore, at time *t*, the system is subject to lateral forces $\mathbf{f}(t)$ and considering that the global force displacement response of the system is defined by a bilinear (or more generally a multilinear) relationship, inelasticity occurs when the sum of the lateral forces in the vector $\mathbf{f}(t)$ exceeds the elastic limit, which is typically defined by a yield force.

The equivalent static force vector $\mathbf{f}(t)$ can be expressed as the superposition of modal forces $\mathbf{f}_n(t)$ as indicated in Eq. (2).

$$\mathbf{f}(t)=\sum\nolimits_n \mathbf{f}_n(t) \tag{2}$$

where the n^{th} mode equivalent static force at time t is given by

$$\mathbf{f}_n(t) = \Gamma_n \mathbf{m}\boldsymbol{\varphi}_n A_n(t) \tag{3}$$

Here, $\Gamma_n = L_n / M_n$, $L_n = \boldsymbol{\varphi}_n^T \mathbf{m}\boldsymbol{\iota}$, $M_n = \boldsymbol{\varphi}_n^T \mathbf{m}\boldsymbol{\varphi}_n$, $\boldsymbol{\varphi}_n$ is the n^{th} mode shape, and the pseudo-acceleration response $A_n(t)$ is represented as follows:

$$A_n(t) = \omega_n^2 D_n(t) \tag{4}$$

where ω_n is the natural circular frequency of the n^{th} mode of vibration and $D_n(t)$ is the displacement response of the n^{th} mode SDOF system obtained by solving Eq. (5) where ς_n is the damping ratio associated with the n^{th} mode.

$$\ddot{D}_n(t) + 2\varsigma_n \omega_n \dot{D}_n(t) + \omega_n^2 D_n(t) = -\ddot{u}_g(t) \tag{5}$$

It is observed from Eq. (3) that the n^{th} mode equivalent static force is the product of two quantities: (1) the time independent term $\Gamma_n \mathbf{m}\boldsymbol{\varphi}_n$ which defines the shape of the force vector and (2) the time-dependent pseudo-acceleration response $A_n(t)$ which defines the amplitude of the shape. The shapes of the first four mode vectors (i.e., $\Gamma_n \mathbf{m}\boldsymbol{\varphi}_n$, n = 1:4) are shown in Fig. 1 for the 35-story building for which the NTHA are conducted in the next section. Because of these shapes, as the pseudo-acceleration response of the 2nd, 3rd or 4th modes increases, these modes provide larger contributions to the equivalent static force vector in Eq. (2), resulting in an increase of the higher mode effects. These contributions are commonly judged by comparing the pseudo-spectral accelerations (PSA) or SA corresponding to the first mode to that of the higher modes since the larger PSA or SA in the higher modes indicates larger higher mode effects according to Eq. (3). However, this approach is not necessarily correct because the pseudo-acceleration response spectrum is based on the maximum value of $A_n(t)$ in Eq. 4, denoted as $A_n(t_{\max})$, when the force vector in Eq. (2) exceeds the elastic limit at a time denoted as t_{yield} before reaching t_{max}, indicating that any linear elastic response computation between t_{yield} and $t_{\max}$ has the potential to provide misleading conclusions about the contribution of the higher mode effects. Accordingly, the MARS proposed in this paper is based on computing the pseudo-acceleration response spectrum using an updated ground motion with duration t_{yield}.

3. Modified Acceleration Response Spectrum

The steps needed to construct the MARS are as follows:

1. Choose a period that will be used for the initial time history analysis and consequent determination of the updated ground motion (T_{inp}). This period should ideally be the first mode period of a structure since the contribution of higher modes are sought to be investigated with respect to the contribution at this period.
2. Choose the base shear coefficient (base shear capacity divided by weight) to be used for the generation of the MARS (η_{inp}).
3. Conduct a linear time history analysis of the SDOF system defined with Eq. 5, with $\omega_n = 2\pi / T_{inp}$ and note the time t_{yield} corresponding to the first occurrence of the following inequality:

$$D_n(t) > \left(\eta_{inp} g\right) / \omega_n^2 \tag{6}$$

where g is the gravitational constant.

4. Compute the MARS using the updated ground motion that has a duration of t_{yield}. Effect of higher modes can be determined by comparing the SA corresponding to the higher mode periods with the SA corresponding to T_{inp}.

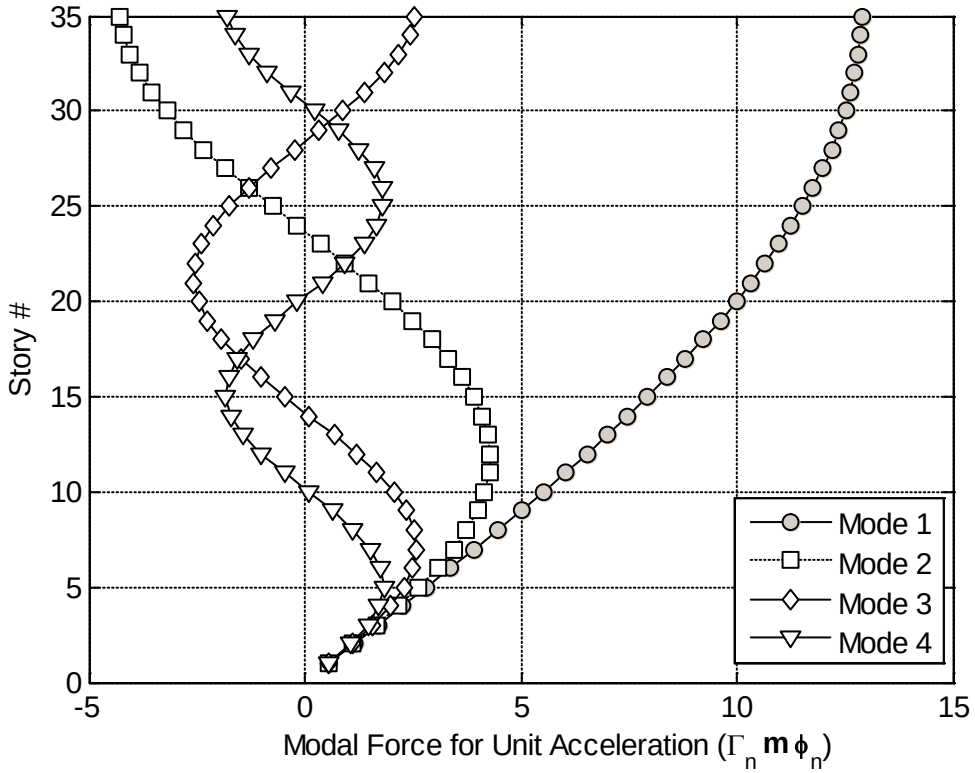

Fig. 1. First four modal force vectors of the 35-story building for unit acceleration

4. Illustrative Application

Since the higher mode effects are more important for tall buildings, the MARS is illustrated using a 35-story building described in [5]. The building has an approximate height of 490-ft with a typical story height of 13-ft and plan dimensions of 185-ft by 135-ft. The structural system of the building is comprised of complete steel moment-resisting space frames with welded connections. The steel frames primarily consist of built-up box (single-cell or two-cell) or wide flange columns welded to beams (either built-up or hot-rolled sections). A typical 6-in.-thick concrete slab on metal deck exists at each floor. The foundation of the building consists of a 7-ft thick mat located 40-ft below grade and supported by more than 2,500 concrete piles that extending to 60-ft below the mat. The foundation mat is connected to a 3-ft thick retaining wall running around the entire foundation [5]. Beam-to-column moment connections incorporate typical pre-Northridge details. Column splices are made of relatively brittle partial joint penetration welds located about 4 ft. from the lower floor level [5]. A perspective view of the building is shown in Fig. 2a.

For the purposes of this study, a simplified model of this 35-story building, Fig. 2b, is developed in OpenSees [6] using spring elements that represent the story force-displacement relationships. The material *Steel01* in OpenSees is used to define these relationships, Fig. 3. The values of the parameters that define these force-displacement relations, namely V_y, k and α, are based on the pushover and eigenvalue analyses conducted in [5]. The first four mode periods of the building are 4.18 sec, 1.40 sec, 0.84 sec, and 0.60 sec. NTHA are conducted on the model using Explicit Newmark integration to avoid convergence problems [7] using 40 ground motions (GMs) selected for a site in Oakland by Baker et al. [8], listed in Appendix A. The ARS and MARS are also developed using OpenSees. However, both spectra can conveniently be developed using custom codes in Matlab, Python, etc. The MARS is computed with T_{inp} = 4.18 sec, which is the first mode period of the structure,

and η_{inp} = 0.1 as documented in [5]. The ground motions that lead to higher mode effects are identified considering the maximum interstory drift (MIDR) distribution along the height. The MARS and ARS are plotted in Figs. 4-9 for these ground motions along with the MIDR distribution obtained from the NTHA. In these figures, it is noted that the computed ARS are scaled to match the SA of the MARS at T_{inp} in order to be able to directly compare the ratios of the SA at the higher modes to the SA at T_{inp} from ARS and MARS.

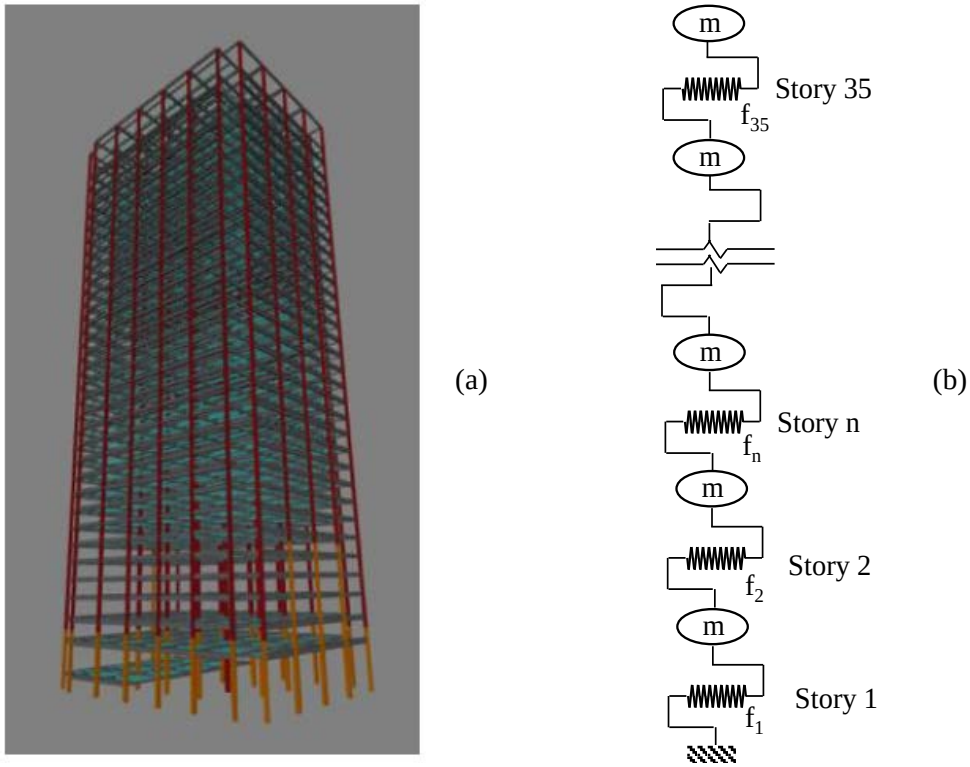

Fig. 2. (a) Perspective view of the 35 story building [5], (b) simplified model used in NTHA

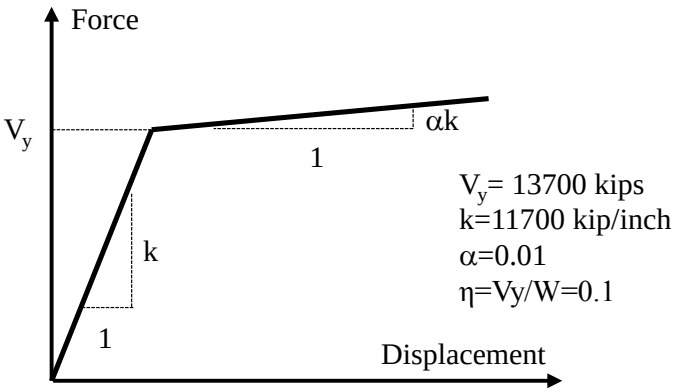

Fig. 3. Story force-displacement relationship of the investigated 35-story building

Some observations from Figs. 4-9 are as follows:

- In all of the cases, the ratios of the higher mode SA to the first mode SA are larger in MARS compared to the ARS.
- The higher mode effect in ground motion 8 (GM8) is identified at story 13. It is observed in Fig. 1 that the second mode force vector has a peak in this story. Therefore, the second mode force contribution is expected to result in a large contribution to the equivalent static force $\mathbf{f}(t)$ before yielding takes place

leading to inelastic response as shown in Fig. 10. It is noted that all of the upper stories marked in Figs. 4-9 are subjected to inelastic response due to higher mode effects. The ratio of the second mode SA to the first mode SA is almost twice larger in MARS compared to ARS. Furthermore, the third and fourth modes also contribute to the equivalent static force, for which the ratio of SA to the first mode SA are significantly larger in MARS in comparison to ARS.

- The higher mode effect in GM25 is detected at story 25. It is observed in Fig. 1 that the fourth mode force vector has a peak in this story. Therefore, the fourth mode force contribution is expected to be responsible for the interstory drift spike in this story. The ratio of the fourth mode SA to the first mode SA is more than twice larger in MARS compared to ARS. Furthermore, the second and third modes also contribute to the higher mode effects, for which the ratio of SA to the first mode SA are significantly larger in MARS in comparison to ARS.
- The higher mode effect in GM31 is observed at story 30. From Fig. 1, all the three higher modes (2nd, 3rd and 4th) provide contributions to the initiation of inelastic response at this story and the ratios of all the higher modes' SA to the first mode SA are larger in MARS compared to those from the ARS.
- The higher mode effect in GM36 occurs at story 27. Similar to GM31, all the three higher mode forces (2nd, 3rd and 4th) in Fig. 1 provide contributions to the initiation of inelastic response at this story and the ratios of all the higher modes' SA to the first mode SA are larger in MARS compared to ARS.
- The higher mode effect in GM39 take place at stories 15 and 25. The fourth mode force vector has peaks both at the 15th and 25th stories in Fig. 1. Therefore, it is likely that the fourth mode is responsible for the higher mode effect at these stories. The effect of the fourth mode on the inelastic response of stories 15 and 25 can also be realized from the force-displacement relationships of these stories in Fig. 10, where it is noted that the yielding of story 15 occurs in one direction while the inelastic response of story 25 occurs in the opposite direction, following the opposite signs of the peaks of the 4th mode force vector in these stories as shown in Fig. 1. The ratio of the fourth mode SA to the first mode SA is 1.5 times larger in MARS compared to ARS.
- The higher mode effect in GM40 takes place at story 28. From Fig. 1, all the three higher modes (2nd, 3rd and 4th) provide contributions to the initiation of inelastic response at this story and the ratios of all the higher modes' SA to the first mode SA are significantly larger in MARS compared to ARS.
- The above observations indicate the superiority of MARS in identifying the higher mode effects compared to ARS.

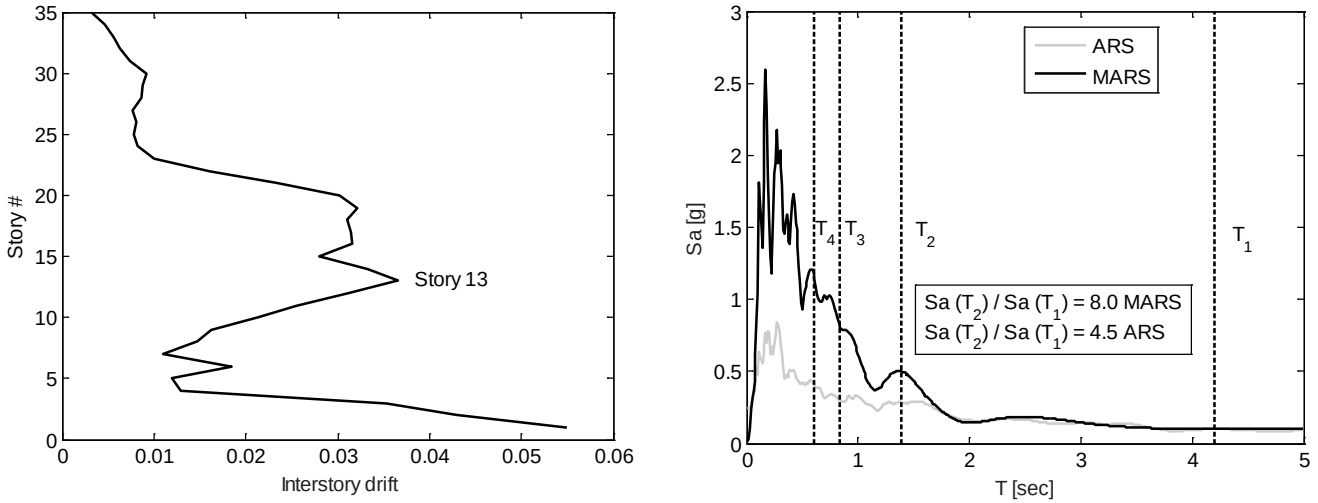

Fig. 4. Maximum interstory drift distribution from NTHA with GM8 (left) and response spectra (right)

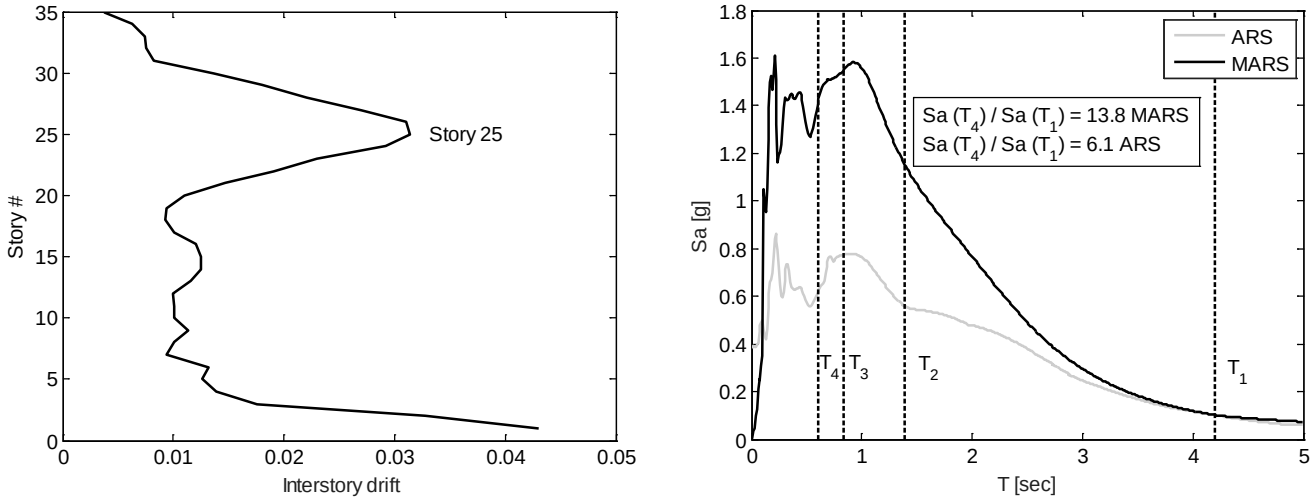

Fig. 5. Maximum interstory drift distribution from NTHA with GM25 (left) and response spectra (right)

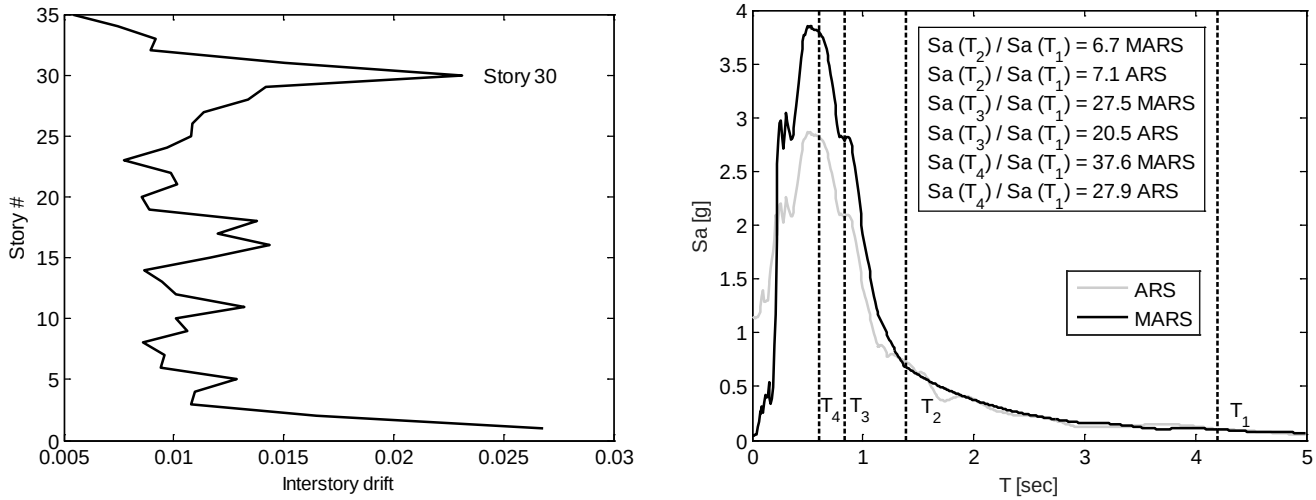

Fig. 6. Maximum interstory drift distribution from NTHA with GM31 (left) and response spectra (right)

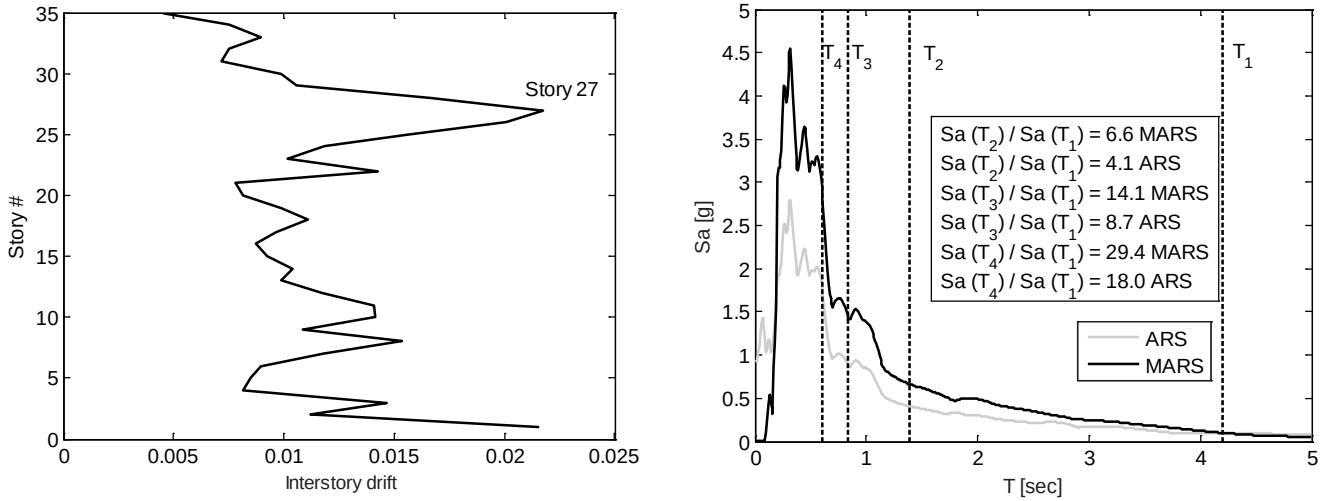

Fig. 7. Maximum interstory drift distribution from NTHA with GM36 (left) and response spectra (right)

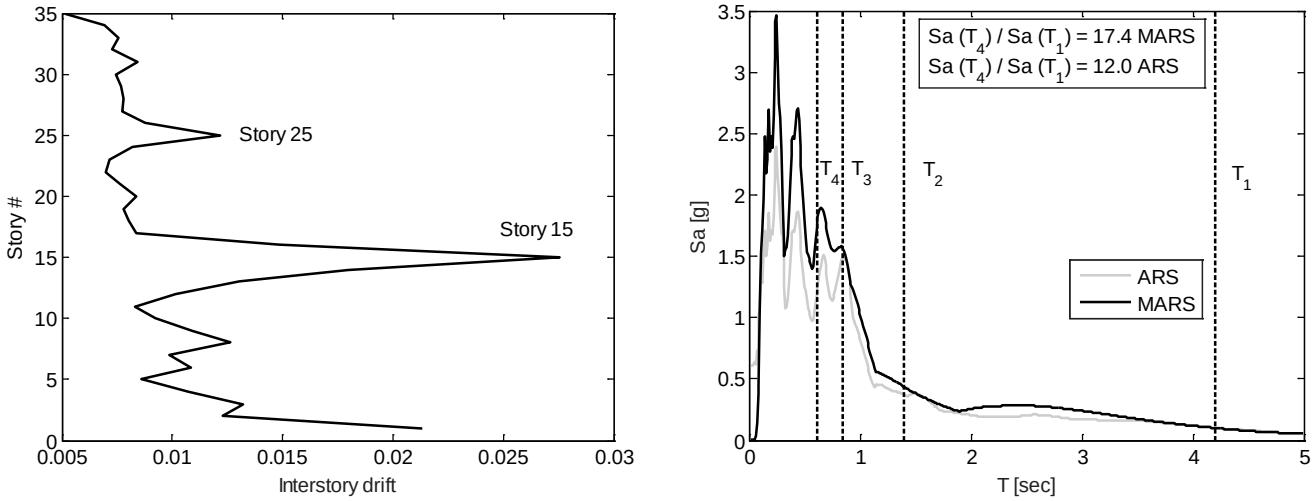

Fig. 8. Maximum interstory drift distribution from NTHA with GM39 (left) and response spectra (right)

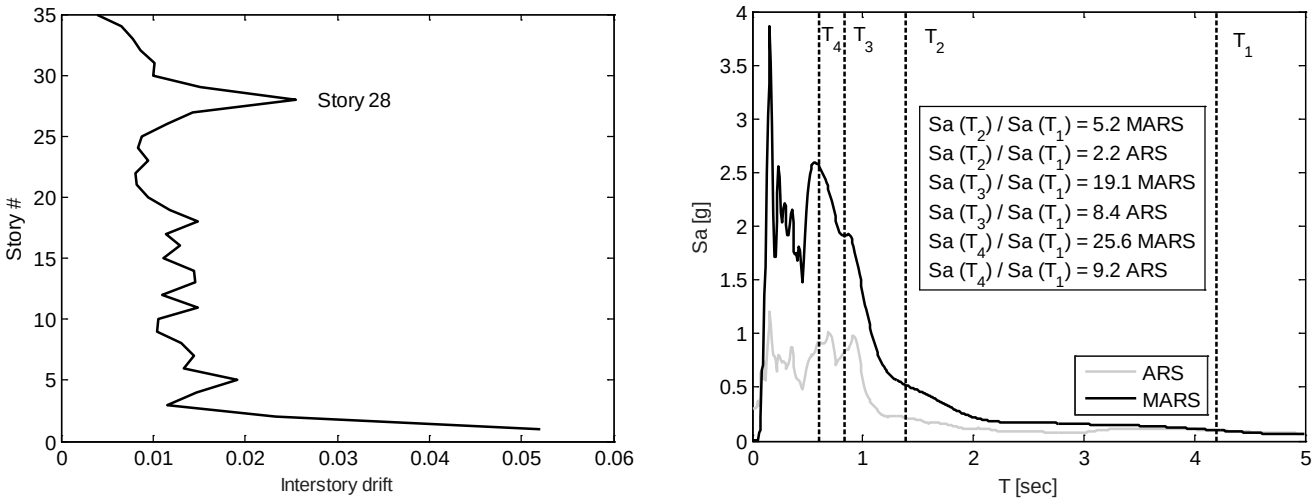

Fig. 9. Maximum interstory drift distribution from NTHA with GM40 (left) and response spectra (right)

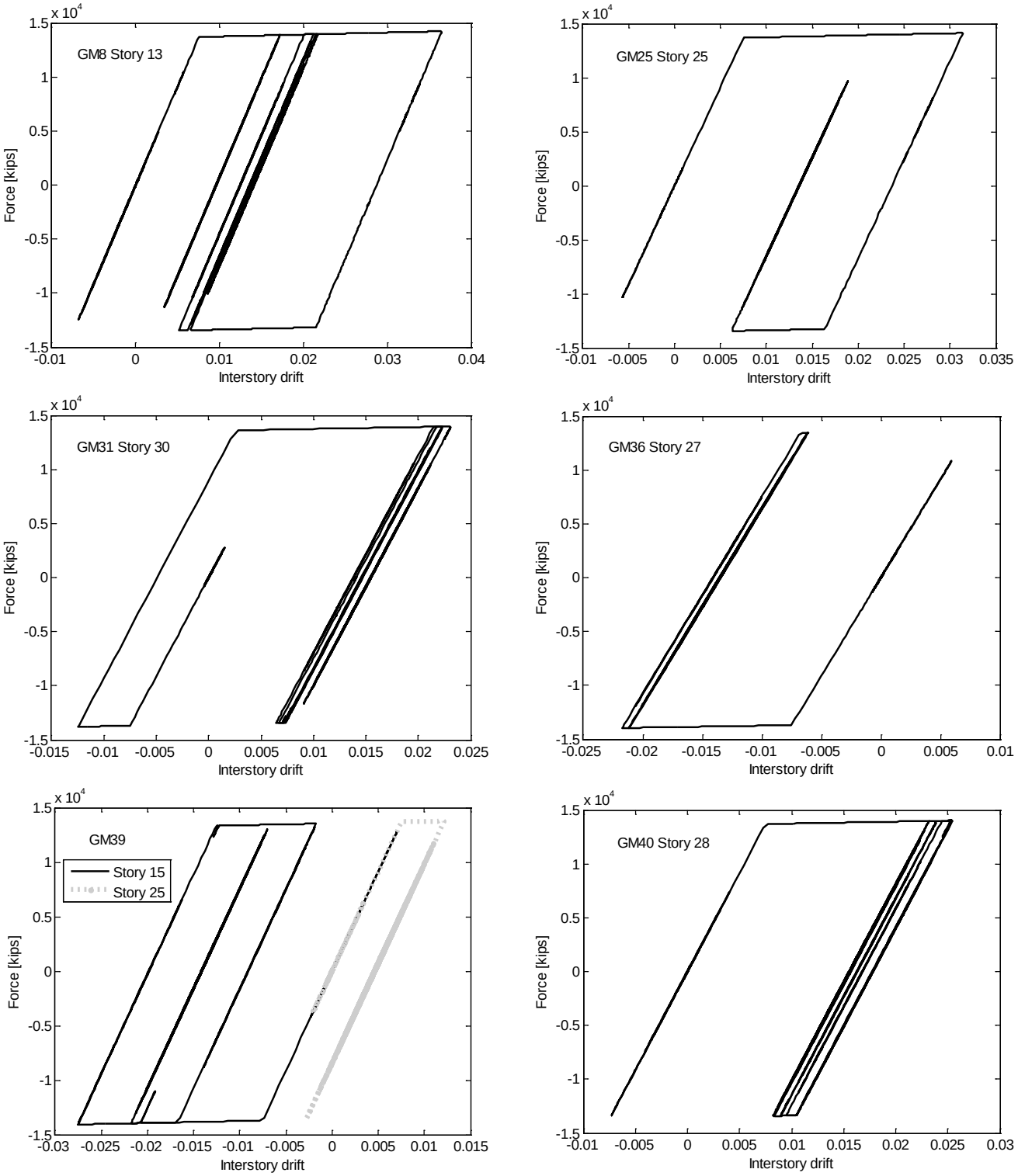

Fig. 10. Inelastic response of upper stories due to higher mode effects

5. Summary and Concluding Remarks

A modified version of the well-known acceleration response spectrum is developed in this paper for improved determination of the higher mode effects. The efficacy of the modified acceleration response spectrum (MARS)

in identifying ground motions that lead to higher mode effects is demonstrated by nonlinear time history analyses conducted on a 35-story building, where the specific observations and conclusions are reported in the previous section. The MARS can easily be developed using existing software or custom codes. Therefore, the benefit introduced by this improved methodology can be conveniently used for identification of higher mode effects. Efficacy of the MARS is planned to be demonstrated for selecting ground motions for buildings with different first mode periods and for different structures, such as bridges, in the near future.

6. References

[1] Housner GW (1941): Calculating the response of an oscillator to arbitrary ground motion, *Bulletin of the Seismological Society of America* **31**, 143–149.

[2] Velestos AS, and Newmark NM (1964): *Response Spectra for Single-Degree-of-Freedom Elastic and Inelastic Systems* Report No. RTD-TDR-63-3096, Vol. III, Air Force Weapons Laboratory, Albuquerque NM.

[3] Riddell R (2008): Inelastic response spectrum: Early history. *Earthquake Engineering & Structural Dynamics*, **37**(8), 1175-1183.

[4] Chopra AK (2006): *Dynamics of Structures: Theory and Applications to Earthquake Engineering*, Pearson Prentice Hall, 3rd Edition, Upper Saddle River, N.J.

[5] Mahin S, Lai JW, Wang S, and Schoettler M (2015): Evaluating and improving the seismic performance of older tall buildings. *Second International Conference on Performance-based and Life-cycle Structural Engineering* (*PLSE 2015*), Dec. 9-11, 2015, Brisbane, Australia.

[6] McKenna F (2010): OpenSees User's Manual, http://opensees.berkeley.edu.

[7] Liang X, Mosalam KM, and Günay, S (2016): Direct integration algorithms for efficient nonlinear seismic response of reinforced concrete highway bridges, *Journal of Bridge Engineering*, 04016041.

[8] Baker JW, Lin T, Shahi SK, and Jayaram N (2011): New ground motion selection procedures and selected motions for the PEER transportation research program, *Technical Report PEER 2011/03*, Pacific Earthquake Engineering Research, Berkeley, USA.

7. Appendix A

Table A-1 – List of employed ground motions [8]

Record #	NGA Record Sequence #	Earthquake Name	Year	Station	Magnitude	Hypo central Distance (km)	Closest Distance (km)	Preferred Vs30 (m/sec)	FN Pulse	Pulse Period (sec)
1	6	Imperial Valley-02	1940	El Centro Array #9	7.0	13.0	6.1	213	0	-
2	159	Imperial Valley-06	1979	Agrarias	6.5	2.6	0.7	275	1	2.30
3	161	Imperial Valley-06	1979	Brawley Airport	6.5	43.2	10.4	209	1	4.03
4	165	Imperial Valley-06	1979	Chihuahua	6.5	18.9	7.3	275	0	-
5	171	Imperial Valley-06	1979	EC Meloland Overpass FF	6.5	19.4	0.1	186	1	3.35
6	173	Imperial Valley-06	1979	El Centro Array #10	6.5	26.3	6.2	203	1	4.49
7	174	Imperial Valley-06	1979	El Centro Array #11	6.5	29.4	12.5	196	1	7.36
8	175	Imperial Valley-06	1979	El Centro Array #12	6.5	32.0	17.9	197	0	-
9	178	Imperial Valley-06	1979	El Centro Array #3	6.5	28.7	12.9	163	1	5.24
10	179	Imperial Valley-06	1979	El Centro Array #4	6.5	27.1	7.1	209	1	4.61
11	180	Imperial Valley-06	1979	El Centro Array #5	6.5	27.8	4.0	206	1	4.05
12	181	Imperial Valley-06	1979	El Centro Array #6	6.5	27.5	1.4	203	1	3.84
13	183	Imperial Valley-06	1979	El Centro Array #8	6.5	28.1	3.9	206	1	5.39
14	184	Imperial Valley-06	1979	El Centro Differential Array	6.5	27.2	5.1	202	1	5.86
15	185	Imperial Valley-06	1979	Holtville Post Office	6.5	19.8	7.7	203	1	4.80
16	187	Imperial Valley-06	1979	Parachute Test Site	6.5	48.6	12.7	349	0	-
17	266	Victoria, Mexico	1980	Chihuahua	6.3	36.7	19.0	275	0	-
18	316	Westmorland	1981	Parachute Test Site	5.9	20.5	16.7	349	1	3.58
19	549	Chalfant Valley-02	1986	Bishop - LADWP South St	6.2	20.3	17.2	271	0	-
20	718	Superstition Hills-01	1987	Wildlife Liquef. Array	6.2	24.8	17.6	207	0	-
21	721	Superstition Hills-02	1987	El Centro Imp. Co. Cent	6.5	35.8	18.2	192	0	-
22	728	Superstition Hills-02	1987	Westmorland Fire Sta	6.5	19.5	13.0	194	0	-
23	768	Loma Prieta	1989	Gilroy Array #4	6.9	32.4	14.3	222	0	-
24	802	Loma Prieta	1989	Saratoga - Aloha Ave	6.9	27.2	8.5	371	1	4.47
25	821	Erzican, Turkey	1992	Erzincan	6.7	9.0	4.4	275	1	2.65
26	949	Northridge-01	1994	Arleta - Nordhoff Fire Sta	6.7	11.1	8.7	298	0	-
27	959	Northridge-01	1994	Canoga Park - Topanga Can	6.7	4.9	14.7	267	0	-
28	982	Northridge-01	1994	Jensen Filter Plant	6.7	13.0	5.4	373	1	3.53
29	1042	Northridge-01	1994	N Hollywood - Coldwater Can	6.7	13.1	12.5	446	0	-
30	1044	Northridge-01	1994	Newhall - Fire Sta	6.7	20.3	5.9	269	0	-
31	1052	Northridge-01	1994	Pacoima Kagel Canyon	6.7	19.3	7.3	508	0	-
32	1063	Northridge-01	1994	Rinaldi Receiving Sta	6.7	10.9	6.5	282	1	1.23
33	1082	Northridge-01	1994	Sun Valley - Roscoe Blvd	6.7	12.4	10.1	309	0	-
34	1085	Northridge-01	1994	Sylmar - Converter Sta East	6.7	13.6	5.2	371	1	3.49
35	1116	Kobe, Japan	1995	Shin-Osaka	6.9	46.0	19.2	256	0	-
36	1602	Duzce, Turkey	1999	Bolu	7.1	41.3	12.0	326	0	-
37	1605	Duzce, Turkey	1999	Duzce	7.1	1.6	6.6	276	0	-
38	2457	Chi-Chi, Taiwan-03	1999	CHY024	6.2	25.5	19.7	428	1	3.19
39	2734	Chi-Chi, Taiwan-04	1999	CHY074	6.2	10.1	6.2	553	0	-
40	2739	Chi-Chi, Taiwan-04	1999	CHY080	6.2	14.5	12.5	553	0	-